Macromolecules

Article

Cite This: Macromolecules 2018, 51, 9222−9233

pubs.acs.org/Macromolecules

Influence of Rubbery versus Glassy Backbone Dynamics on Multiscale Transport in Polymer Membranes

Kevin Chang,[†] Andrew Korovich,[‡] Tianyi Xue,[†] William A. Morris,[†] Louis A. Madsen,[‡] and Geoffrey M. Geise*[,†]

[†]Department of Chemical Engineering, University of Virginia, Charlottesville, Virginia 22903, United States

[‡]Department of Chemistry and Macromolecules Innovation Institute, Virginia Tech, Blacksburg, Virginia 24061, United States

Supporting Information

ABSTRACT: To determine the effects of polymer backbone dynamics on water and salt permeation in water purification membranes, we investigate the fundamental transport and sorption properties of two series of chemically similar copolymers: methacrylate-based copolymers that are glassy at room temperature and acrylate-based copolymers that are rubbery at room temperature. Water diffusion measurements made as a function of diffusion time using pulsed-field-gradient NMR diffusometry provide information about hydrophilic network heterogeneity in the copolymers. These time-dependent measurements enable us to parse tortuosity into two regimes, the nanometer-to-bulk and micrometer-to-bulk ranges, enhancing insight into the influence of copolymer morphology on bulk transport. Combining NMR diffusometry and water and salt sorption and transport measurements, we find that the glassy methacrylate copolymers exhibit greater water−salt selectivity than the acrylate copolymers. These differences likely arise from sub-micrometer polymer morphological and dynamical differences, and we propose multiscale models for heterogeneities of the hydrophilic networks in these copolymers.

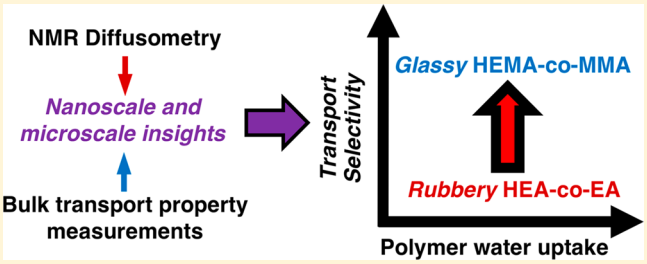

1. INTRODUCTION

Polyamide-based reverse osmosis and nanofiltration membranes are the current state-of-the-art[1−4] in water purification systems used to help address global water shortages.[1−7] Polyamide materials, however, are susceptible to oxidative degradation via chlorine-containing compounds present after necessary pretreatment of feedwater, and therefore advanced chlorine-tolerant membrane polymers are needed.[1,3,6,8−10] While others have produced chlorine-tolerant polymers from polysulfone and poly(phenylene oxide),[9−11] a combination of chlorine tolerance and favorable selectivity properties remains elusive. Thus, structure−property relationships are needed to guide engineering of advanced membrane polymers with the necessary combination of properties to purify water efficiently and effectively.[6,12−15]

Polyamide-based commercial desalination membranes sorb only around 10% water by mass,[16,17] in contrast to commercial ion exchange materials, such as Nafion, that can sorb up to about 30% water.[18] In high water content materials such as Nafion, water molecule dynamics play a key role in governing water and salt transport properties.[19−23] In lower water content polymers, interactions between water molecules and the polymer backbone are more significant compared to that in highly hydrated materials, so backbone structure and dynamics will tend to influence transport properties to a greater extent in low water content polymers. We have previously reported glassy polymers that show greater salt permeability and diffusion selectivity than comparable rubbery polymers at equivalent water content.[24] Questions still remain about the influence of water dynamics, backbone dynamics, and polymer structure on water and salt transport properties, which are critical for water purification applications, of glassy versus rubbery low water content polymers at equivalent water content.

To address these questions, two series of chemically similar low water content copolymers were studied at room temperature: a glassy methacrylate-based copolymer (HEMA-*co*-MMA) and a rubbery acrylate-based copolymer (HEA-*co*-EA).[24] The glassy methacrylate polymer was expected to have slower segmental dynamics compared to the acrylate polymer that was rubbery at room temperature. Bulk transport properties of these copolymers were compared at equivalent water content since water and salt transport properties are highly sensitive to water sorption.[3,6,7,25]

Pulsed-field-gradient NMR diffusometry offers detailed insight into water transport dynamics inside polymer systems. By varying the experimental diffusion time, we find that in both series of copolymer membranes the diffusion coefficient of water decreases as the diffusion time increases, signifying the presence of structural heterogeneity on the micrometer length scale probed by the NMR diffusometry experiment. This phenomenon is also known as restricted diffusion,[26] which has

Received: August 24, 2018
Revised: October 24, 2018
Published: November 8, 2018

DOI: 10.1021/acs.macromol.8b01830
Macromolecules 2018, 51, 9222−9233

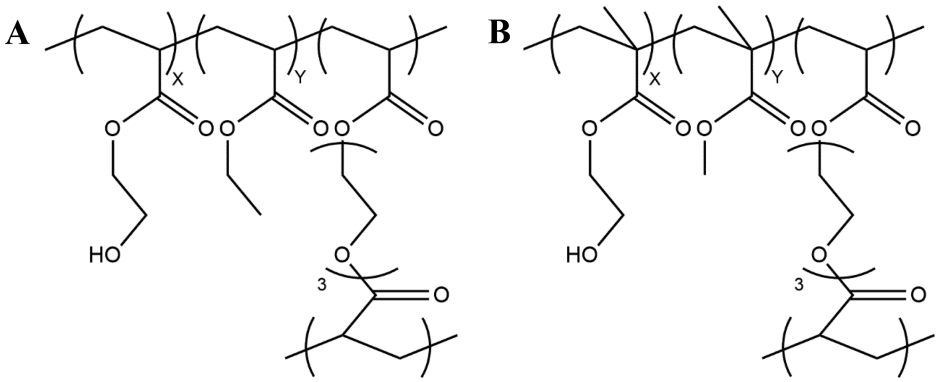

Figure 1. (A) HEA-*co*-EA and (B) HEMA-*co*-MMA random copolymers for investigation of water and salt transport properties. The ratios of hydrophilic to hydrophobic comonomers are represented on each structure as mass percentages (e.g., the HEA-*co*-EA material contained an *X*:*Y* (by mass) ratio of HEA:EA). Because of differences in the hydrophilicity of the monomer units, we expect some degree of nanophase separation of the hydroxyl (and possibly ester) groups from the backbone and alkyl side chains. This nanophase separation may be more kinetically trapped or sharper in the more rigid HEMA-*co*-MMA copolymers than in the HEA-*co*-EA copolymers, where more flexible backbone dynamics may smooth out these nanoscale structural features.

been previously used to understand heterogeneity and transport in porous media[27] including polymeric systems.[28] Furthermore, we extract two separate tortuosity values, from these measurements, that correspond to averaging over different length scales (from the nanometer-to-bulk and micrometer-to-bulk) of transport resistance. We use these tortuosity parameters to better understand differences in water diffusion due to multiscale polymer morphology. We find that the micrometer-to-bulk tortuosity is similar between both series of copolymers, while the nanometer-to-bulk tortuosity is 5 times larger in the glassy compared to the rubbery copolymers, suggesting that the rigid backbone of the methacrylate copolymer results in a more tortuous hydrophilic network that slows the overall water transport through the copolymer.

Upon combining NMR diffusometry results with bulk sorption and transport measurements, we found that the methacrylate-based polymers were more water/salt selective than the acrylate-based polymers due to salt diffusivity properties that are suppressed to a greater extent than the water diffusivity properties in the methacrylate polymers. Therefore, the formation of more rigid and tortuous transport pathways in the glassy methacrylate polymers likely hinders transport of larger hydrated ions to a greater extent than the smaller water molecules and increases water/salt selectivity compared to the rubbery acrylate polymers. In low water content polymers, the use of rigid backbone segments to generate selective nanoscale polymer features may be a viable strategy for increasing the water/salt selectivity of polymers for water purification applications.

2. EXPERIMENTAL SECTION

2.1. Materials. Two series of chemically similar copolymers were prepared so that one series would have a flexible backbone and the other series would have a rigid backbone at room temperature. An acrylic copolymer composed of 2-hydroxyethyl acrylate (HEA, 96%, Sigma-Aldrich) and ethyl acrylate (EA, 99%, Sigma-Aldrich) comonomers was chosen as the flexible backbone polymer, and the rigid backbone material was chosen to be a methacrylate-based copolymer and was composed of 2-hydroxyethyl methacrylate (HEMA, 97%, Sigma-Aldrich) and methyl methacrylate (MMA, 99%, Sigma-Aldrich) comonomers. Poly(ethylene glycol diacrylate) (PEGDA, average M_n = 250 g mol^{-1}, Sigma-Aldrich) was used as a cross-linker. The methacrylate backbone copolymer was expected to be more rigid than the acrylic copolymer because of the extra methyl group on the methacrylate backbone that increases the energy barrier for chain rotation.[24]

Copolymers were prepared by mixing the comonomers, cross-linker, and a UV photoinitiator (1-hydroxycyclohexyl phenyl ketone, HCPK, 99%, Sigma-Aldrich) to form a prepolymerization solution. This solution was stirred for 10 min to form a homogeneous mixture and then sonicated for 15 min in an ultrasonic water bath to degas the solution. Then, the prepolymerization solution was confined between a quartz plate and a glass plate and irradiated with 120 μJ/cm^2 of 254 nm UV radiation to form clear and transparent films using free radical polymerization. Film thickness was controlled by stainless steel spacers that were used to separate the quartz and glass plates during the curing process. Typical final film thicknesses were in the range 50−200 μm.

Three compositions of each copolymer were prepared. Sample nomenclature is based on the hydrophilic comonomer (i.e., HEA or HEMA) and hydrophobic comonomer (i.e., EA or MMA). Thus, the flexible copolymer is designated HEA-*co*-EA *X*:*Y*, and the rigid copolymer is designated HEMA-*co*-MMA *X*:*Y*. The prepared compositions (*X*:*Y* = 30:70, 35:65, or 40:60) represent the mass ratios of the hydrophilic comonomer to hydrophobic comonomer. All copolymers were cross-linked using 3% (by mass relative to the total mass of the hydrophilic and hydrophobic comonomers) PEGDA (Figure 1), and the HCPK initiator concentration in the prepolymerization solution was 0.5% and 1% (by mass) for HEA-*co*-EA and HEMA-*co*-MMA, respectively. The curing times were 120 and 500 s for the HEA-*co*-EA and HEMA-*co*-MMA materials, respectively. After curing, the clear and transparent films were soaked promptly in deionized (DI) water (18.2 MΩ cm and 1.2 ppb total organic carbon) to hydrate the copolymers. Films prepared for salt transport and pulsed field gradient NMR measurements were transferred to and allowed to equilibrate with 0.5 mol/L aqueous sodium chloride (NaCl) solution prior to characterization.

2.2. Methods. *Water Uptake.* The equilibrium water content of the copolymers was characterized as the gravimetric water uptake (mass of water sorbed in the polymer per mass of dry polymer). First, samples were equilibrated with either DI water or 0.5 mol/L aqueous sodium chloride (NaCl, ≥99%, Sigma-Aldrich) solution for at least 24 h at room temperature. The hydrated sample mass, m_{wet}, was measured rapidly after removing the sample from the initial equilibration solution and wiping the surface of the film with a laboratory wipe to remove excess solution from the surface. Then, the sample was placed in a vented Petri dish and dried under vacuum at room temperature for 48 h.[24] This drying time was found to be sufficiently long to ensure that the mass of the polymer stabilized to the dry polymer mass, m_{dry}.To minimize the effects of atmospheric moisture sorption on the dry polymer mass, the vacuum oven was

DOI: 10.1021/acs.macromol.8b01830
Macromolecules 2018, 51, 9222−9233

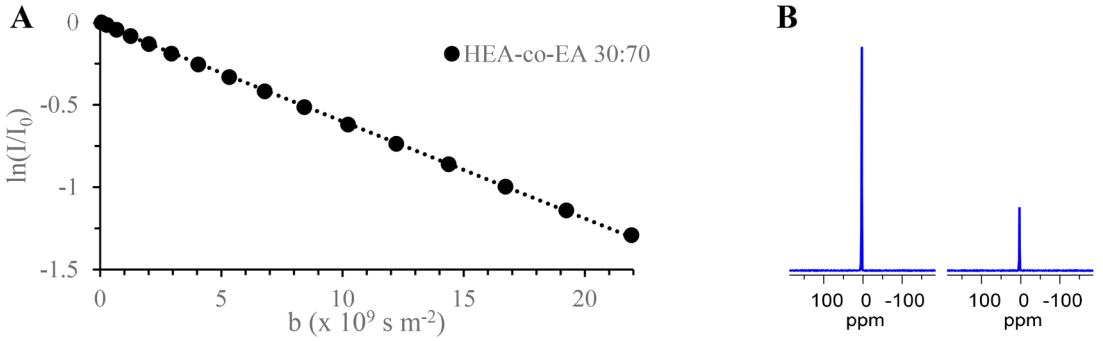

Figure 2. Measuring water diffusion with NMR diffusometry. The linearized signal attenuation plot (A) for fully hydrated HEA-*co*-EA 30:70 at 298 K shows the attenuation of the normalized NMR signal intensity as a function of the Stejskal−Tanner parameter, b (eq 4). The slope of the data is equal to the self-diffusion coefficient of water in the polymer, which is 5.6×10^{-8} cm^2/s in this example. NMR diffusometry signal attenuation, from the first to the last measurement, can be seen in the 1D spectra (slices) from the experiment (B), which are from the first and last (g_{max} = 300 G/cm) point in (A).

filled with dry air (using a Drierite column) prior to removing samples from the oven for the dry mass measurement. This approach blanketed samples in the Petri dishes with dry air prior to the dry mass measurement. The water uptake, w_u, was calculated as

$$w_u = \frac{m_{wet} - m_{dry}}{m_{dry}} \quad (1)$$

Reported water uptake values are the average of four measurements, and the uncertainty in w_u was taken as one standard deviation from the mean.

The volume fraction of water sorbed in the membrane, ϕ_w^m, was calculated, using an assumption that volumetric mixing of water and polymer is additive (see the Supporting Information), as

$$\phi_w^m = \frac{w_u}{w_u + \rho_w/\rho_p} \quad (2)$$

where ρ_w and ρ_p are densities of water (taken as 1.0 g cm^{-3})[29] and dry polymer, respectively.[30,31] The dry polymer density was measured using an Archimedes' principle method (Mettler Toledo, 11106706).[24,32,33] Cyclohexane was used as the auxiliary liquid for the density measurement.[24,34] Uncertainty in the volume fraction of water sorbed by the polymer was determined using standard error propagation techniques.[35]

The water sorption coefficient, K_w, is defined as the ratio of water concentration in the polymer, C_w^m, to that in bulk external solution, C_w,[36−38] and the units of K_w are [g(water)/cm^3(hydrated polymer)]/[g(water)/cm^3(solution)]. The water sorption coefficient was calculated using the measured volume fraction of water in the polymer, ϕ_w^m, as[39]

$$K_w = \frac{C_w^m}{C_w} = \frac{\phi_w^m M_w}{C_w^s \bar{V}_w} \quad (3)$$

where M_w is the molar mass of water (18 g mol^{-1}), C_w^s is the concentration of water in the bulk solution, which was taken as 1.0 g cm^{-3},[39] and $\bar{V}_w$ is the partial molar volume of water in the polymer (taken as 18 cm^3 mol^{-1}).[40,41] Evaluating eq 3 reveals that the water sorption coefficient is effectively equivalent to the volume fraction of water sorbed in the polymer.[42]

Thermal Characterization. The glass transition temperature, T_g, of the hydrated copolymers was characterized using differential scanning calorimetry (DSC) (TA Instruments Q1000). Polymer samples were equilibrated with DI water, cut into small pieces, and sealed in hermetic aluminum pans such that ∼5−10 mg of sample was placed in each pan. Hermetic pans were used to keep the samples hydrated throughout the DSC measurement.

Samples were initially heated to 150 °C to erase thermal history.[43] Then, the samples were quenched to −80 °C and subsequently heated to 150 °C at 10 °C/min. The sample chamber of the calorimeter was continuously purged with dry nitrogen throughout the experiment, and no evidence of water vaporization was observed during the first heating ramp, suggesting that the hermetic pans were well sealed. The glass transition temperature was determined to be the midpoint of the step change in the heat flow versus temperature curve.[44]

NMR Sample Preparation and Diffusometry. HEA-*co*-EA samples were prepared for NMR by first cutting 8−32 circular (3 mm in diameter) pieces of polymer. The final number of pieces of polymer used was chosen to ensure that the NMR signal was sufficiently strong during the measurement. Similarly, the HEMA-*co*-MMA samples were prepared by cutting approximately 3 mm × 4 mm pieces of polymer. Rectangular pieces of HEMA-*co*-MMA were used in contrast to the circular HEA-*co*-EA samples because the HEMA-*co*-MMA samples were too brittle to cut using a circular die. These slices were stacked and wrapped with thin strips of PTFE tape to hold them together and were equilibrated in 0.5 mol/L NaCl solutions for at least 72 h prior to NMR experiments. Then, stacked samples were removed from solution, quickly blotted to remove surface water, wrapped completely in PTFE tape, and placed into a sealed poly(methyl methacrylate), PMMA, sample cell. The sample cell was designed to have a very small amount of excess volume to minimize water loss during NMR data collection.[45]

The ^1H_2O self-diffusion measurements were made using a pulsed-gradient stimulated echo (PGSTE) sequence at 25 °C on a Bruker Avance III 9.4T wide-bore spectrometer. A single axis diffusion probe (Bruker Diff60) was used with a 5 mm ^{1}H radio-frequency coil. The Stejskal−Tanner equation describes the signal attenuation that results from diffusion in the PGSTE experiment:

$$I = I_0 e^{-D_w \gamma^2 g^2 \delta^2 (\Delta - \delta/3)} = I_0 e^{-bD} \quad (4)$$

where I is the signal intensity at a given gradient strength, g (maximum gradient strengths ranged from 100 to 800 G/cm), I_0 is the signal intensity at g = 0 G/cm, D_w is the water diffusion coefficient, γ is the gyromagnetic ratio of the ^{1}H nucleus (267.522 rad s^{-1} T^{-1}), δ is the effective rectangular gradient pulse length (2 ms), Δ is the diffusion encoding time (values ranged from 8.2 to 750 ms), and b is the Stejskal−Tanner parameter.

The water diffusion coefficient, D_w, was obtained by fitting the I/I_0 data, obtained from a PGSTE experiment, as a function of g. An example signal attenuation curve for HEA-*co*-EA 30:70 is shown in Figure 2. In the PGSTE experiments, a 90° radio-frequency pulse of 4.8 μs was used with 16 gradient steps (8−128 scans per step with a repetition time of 2−3 s). The 16 gradient step experiment was needed to deconvolute a fast diffusion coefficient component, which was attributed to the small amount of residual surface water on the sample, and a slower diffusion coefficient component, which was attributed to water sorbed in the polymer. Transverse relaxation times, T_2, for water signals in these polymers ranged from 1 to ∼50 ms, and the longitudinal relaxation times, T_1, ranged from 700 to 750 ms.

DOI: 10.1021/acs.macromol.8b01830
Macromolecules 2018, 51, 9222−9233

Table 1. Dry Polymer Density and Water Content Data (Water Uptake, w_u, and Water Sorption Coefficient, K_w; Compare Eqs 1 and 3), Determined Using Both Aqueous NaCl Solution (0.5 mol/L) and Pure (DI) Water, for the Three Compositions of Each Copolymer[a]

			measured using 0.5 mol/L NaCl		measured using DI water	
copolymer	composition[b]	dry polymer density [g/cm^3]	w_u[c]	K_w	w_u[c]	K_w
HEA-*co*-EA	30:70	1.20 ± 0.01	0.074 ± 0.006	0.081 ± 0.006	0.081 ± 0.006	0.089 ± 0.007
	35:65	1.20 ± 0.01	0.082 ± 0.004	0.090 ± 0.004	0.091 ± 0.005	0.098 ± 0.005
	40:60	1.22 ± 0.01	0.102 ± 0.008	0.109 ± 0.009	0.171 ± 0.007	0.170 ± 0.007
HEMA-*co*-MMA	30:70	1.22 ± 0.01	0.086 ± 0.004	0.095 ± 0.004	0.091 ± 0.005	0.100 ± 0.006
	35:65	1.23 ± 0.01	0.091 ± 0.005	0.100 ± 0.006	0.098 ± 0.003	0.107 ± 0.003
	40:60	1.25 ± 0.02	0.115 ± 0.003	0.126 ± 0.003	0.192 ± 0.008	0.190 ± 0.008

[a]All data were measured at room temperature, and the uncertainties are reported as one standard deviation from the mean value. [b]Copolymer compositions are reported as hydrophilic (e.g., HEA or HEMA):hydrophobic (e.g., EA or MMA) comonomer content (by mass). [c]Water uptake units: g(water)/g(dry polymer).

Salt Sorption. The salt sorption coefficient, K_s (defined as the ratio of salt concentration in a hydrated polymer, C_s^m, at equilibrium to that in the external solution, C_s^s), was measured using a desorption procedure.[24] First, a hydrated sample was immersed in 0.5 mol/L aqueous sodium chloride solution and allowed to reach equilibrium. The necessary time for this process was estimated as the characteristic time of the diffusion process, L^2/D_s, where D_s is the average diffusion coefficient of salt in the hydrated polymer and L is the diffusion path length (i.e., half of the sample thickness).[46] As the values of D_s were unknown prior to the measurement, they were estimated to be ~10 h using the Mackie and Mears model, which describes the diffusivity in the polymer as a function of the volume fraction of water in the hydrated polymer.[47] Therefore, samples were equilibrated in salt solution for at least 3 days (more than 7 times the characteristic diffusion time) prior to the desorption measurement.

After equilibration in salt solution, the sample volume, V_p, was determined by measuring the surface area and thickness of the sample. Then, the sample was transferred into DI water to allow sorbed salt to desorb from the polymer. The volume of the desorption solution, V_d, was chosen iteratively such that the final salt concentration in the solution was ~1 mg(salt)/L. This choice ensured that the salt concentration was sufficiently low to facilitate complete desorption of salt from the sample but was high enough to be measured accurately.[48] The concentration of salt in the desorption solution, C_d, was measured using ion chromatography (ICS-2100, Thermo Scientific). The salt sorption coefficient was calculated as

$$K_s = \frac{C_s^m}{C_s^s} = \frac{C_d V_d}{C_s^s V_p} \tag{5}$$

Salt Diffusion. The effective salt diffusion coefficient, D_s, was determined by measuring the initial salt desorption from a salt solution-equilibrated polymer as a function of time. Fickian diffusion analysis provides a relationship between the mass of desorbed salt, M_t, as a function of time, t, that can be simplified for the case where the ratio of M_t to M_∞, which is the mass of salt desorbed from the polymer at infinite time, is less than 0.6:[49]

$$\left.\frac{M_t}{M_\infty}\right|_{M_t/M_\infty<0.6} = \left(\frac{16D_s}{\pi L^2}\right)^{1/2} t^{1/2} \tag{6}$$

where L is the sample thickness, which was determined using the measured sample area and thickness.

Samples were initially equilibrated in 0.5 mol/L aqueous NaCl solution (per the procedure described earlier for the salt sorption measurement). The sample surface was carefully dried with a laboratory wipe prior to the desorption to remove any residual salt solution from the surface. The desorption solution (DI water) was atmospherically equilibrated so that solution conductivity changes, due to absorption of atmospheric carbon dioxide, would not influence the measurement.[39] The desorption solution was maintained at 25 °C using a temperature-controlled water circulator and was kept well mixed using a magnetic stir bar.[39,50] The conductivity of the desorption solution was measured as a function of time (using a Cond 7310, WTW, Germany conductivity meter) and converted to salt mass, M_t, using a calibration curve and the desorption solution volume.

3. RESULTS AND DISCUSSION

3.1. Material Selection. A critical component of this study was the preparation of low water content polymers with different segmental dynamics and similar chemistry. To accomplish this task, copolymers were prepared using chemically similar HEA, HEMA, EA, and MMA comonomers.[24] In order for the membranes to have comparable water uptake to commercial desalination membranes (10% by mass), we used hydrophobic comonomers (EA and MMA) to balance the highly hydrophilic HEA and HEMA monomers.[16]

3.2. Water Content. We controlled copolymer water content using the ratio of hydrophilic comonomer (i.e., HEA 316 or HEMA) to hydrophobic (i.e., EA or MMA) comonomer. The water uptake (w_u) and water sorption coefficient (K_w) values for both copolymers increased as the hydrophilic comonomer composition increased from 30% to 40% (by mass) (Table 1). To enable accurate comparison of transport properties between the copolymers, we controlled the copolymer hydrophilicity such that the water uptake of the two copolymer series overlapped. Comparing materials at equivalent water content is critical, as water and salt transport in polymers is strongly influenced by water content.[25] Additionally, the water content of samples initially equilibrated in 0.5 mol/L sodium chloride was lower than that of materials equilibrated in deionized (DI) water (Table 1) because of osmotic deswelling due to the lower thermodynamic activity of water in the salt solution.[6,51]

The polymer water content was analyzed in terms of the amount of water available to hydrate the hydrophilic moieties within the polymer to provide insight into the hydrogen bonding environment within the polymer. We combined measured water uptake data with polymer composition information to calculate the molar ratio (equivalents) of water sorbed in the polymer to both −OH and −O− functional groups in the copolymers. These calculations (results in the Supporting Information) indicate that the polymer with the highest water uptake, HEMA-*co*-MMA 40:60, sorbs 2 equiv of water per total equivalents of −OH and −O−, and the polymer with the lowest water uptake, HEA-*co*-EA 30:70, sorbs 1.5 equiv of water per total equivalents of −OH and −O−. These calculations suggest

DOI: 10.1021/acs.macromol.8b01830
Macromolecules 2018, 51, 9222−9233

that the majority of the sorbed water in these copolymers interacts with the polymer backbone to some extent.

3.3. Salt Sorption Properties. The HEA-*co*-EA and HEMA-*co*-MMA salt sorption coefficients appear to overlap as a function of water uptake (Figure 3). Salt sorption in uncharged polymers is expected to be primarily dependent on water uptake and the chemical structure of the polymer,[52] so it is reasonable that copolymers with similar chemistry and water content exhibit similar salt sorption properties. The results shown in Figure 3 suggest that the chemical environment of both copolymers is similar to the point where salt sorption properties appear to be unaffected by subtle differences in chemical structure. The practical implication of this result is that differences in transport properties between the two copolymers, compared at equivalent water content, can be attributed to kinetic or diffusion-related phenomena as opposed to thermodynamic or sorption phenomena.

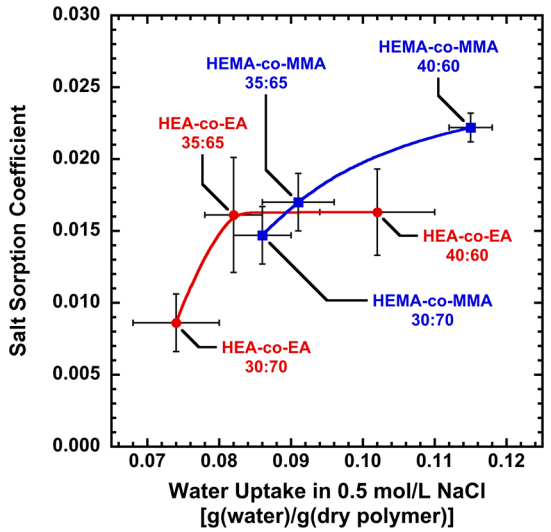

Figure 3. Salt sorption coefficient, K_s, data for HEA-*co*-EA and HEMA-*co*-MMA copolymers as a function of water uptake in 0.5 mol/L NaCl solution. Sorption data were measured after equilibrating samples in 0.5 mol/L NaCl at room temperature. The uncertainty in the data was taken as one standard deviation from the mean of four measurements.

3.4. Polymer and Water Dynamics. The hydrated HEMA-*co*-MMA copolymers had glass transition temperature, T_g, values that were above room temperature, and the hydrated HEA-*co*-EA copolymers had T_g values that were below room temperature (Figure 4). This result suggests that the segmental dynamics in the HEMA-*co*-MMA copolymers were slower compared to the HEA-*co*-EA copolymers, as the glass transition temperature can be interpreted as the temperature at which sufficient thermal energy has been provided to the polymer to facilitate segmental motion. Below T_g, polymer chains are kinetically trapped, but above T_g, the polymer chains can relax.[53]

This result is likely due to steric hindrance of the methyl groups on the methacrylate backbone that increase the energy barrier for segmental motion compared to acrylate backbones.[54] This connection between T_g and segmental dynamics is significant because, at room temperature, segmental dynamics in the glassy HEMA-*co*-MMA copolymer are expected to be slower compared to the rubbery HEA-*co*-EA copolymers.[8] In other words, at room temperature, the HEMA-*co*-MMA backbone is expected to be rigid compared to the more flexible HEA-*co*-EA backbone.

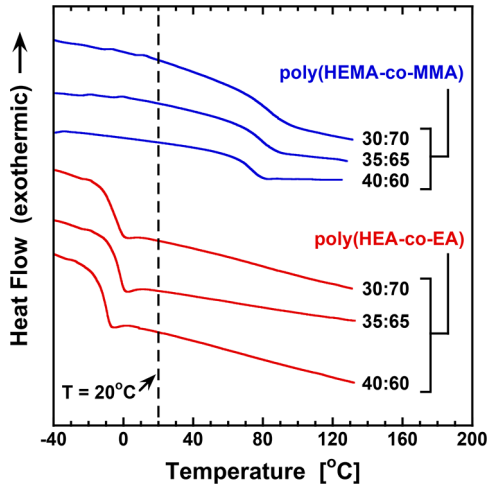

Figure 4. Second scan DSC thermograms for hydrated poly(HEMA-*co*-MMA) and poly(HEA-*co*-EA) samples. Sealed hermetic aluminum pans were used to maintain sample hydration, and the heating rate was 10 °C/min. The thermograms are displaced vertically for clarity, and the compositions of the copolymers are listed as the ratio of hydrophilic to hydrophobic comonomer (by mass).

We prepared both series of copolymers using PEGDA as the cross-linker, and due to the differing reactivity of the methacrylate comonomers and the PEGDA acrylate groups compared to the situation for the acrylate comonomers, copolymers may not be statistically random. Thermal analysis, however, does suggest a high degree of molecular mixing because a single T_g is observed for all of the copolymers, and this result contrasts other copolymer compositions that were closer to 50:50 and exhibited two distinct glass transitions (data not reported here). Furthermore, we compared T_g values calculated from the Fox equation (based on T_g's of the copolymer components) to the measured T_g values (Table 2).[24,55,56] We report details of this calculation elsewhere[24]

Table 2. Glass Transition Temperatures Calculated Using the Fox Equation[24] and the Measured Glass Transition Temperatures (Figure 4) for the Copolymers

		T_g [°C]	
copolymer	composition	Fox equation	measured
HEA-*co*-EA	30:70	−22	−20
	35:65	−21	−19
	40:60	−22	−22
HEMA-*co*-MMA	30:70	100	90
	35:65	97	88
	40:60	105	80

where we observed relatively good agreement between measured and calculated T_g values. These results suggest the absence of significant phase separation and good incorporation of the cross-linker, but differences in reactivity and the hydrophilicity of the comonomers may still lead to heterogeneity over sufficiently small length scales.

The DSC thermograms (Figure 4) do not show strong evidence of free or bulk water (i.e., melting transitions at 0 °C). This point on the HEA-*co*-EA thermograms is obscured by the glass transition, but the absence of a strong melting

DOI: 10.1021/acs.macromol.8b01830
Macromolecules 2018, 51, 9222−9233

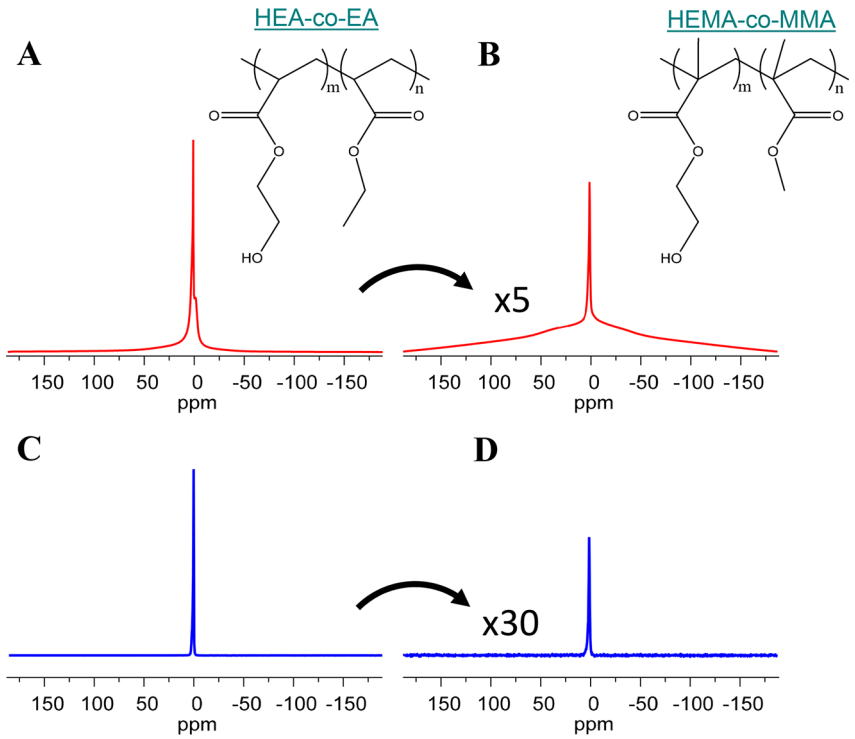

Figure 5. ^{1}H NMR spectra that illustrate water and polymer spectral components in 1D and in diffusometry experiments for HEA-*co*-EA 30:70 and HEMA-*co*-MMA 30:70 equilibrated in 0.5 mol/L NaCl solution. Plots A and B are 1D pulse-acquire NMR spectra (32 scans each), and spectra C and D were obtained from the first gradient step (smallest g) of the NMR diffusometry experiment (16 scans each). The signal from the HEMA-*co*-MMA measurements was weak compared to that from HEA-*co*-EA, so the vertical scales of the B and D spectra have been multiplied by scaling factors to illustrate peak shapes more clearly.

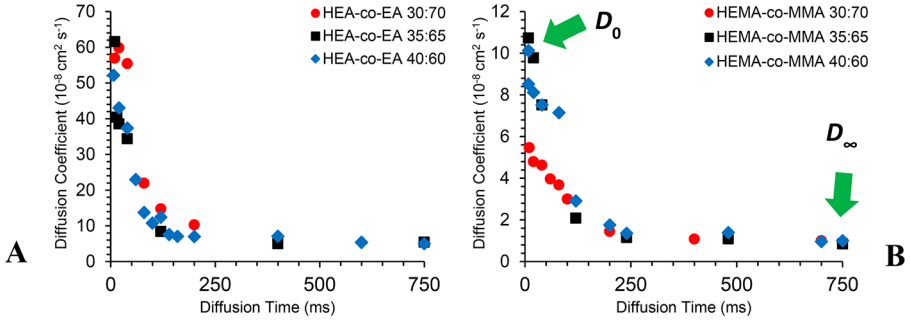

Figure 6. Water diffusion coefficients, D_w, decrease as diffusion time, Δ (and diffusion length, l_d), increase in both the (A) HEA-*co*-EA and (B) HEMA-*co*-MMA copolymers. We define D_0 as the water diffusion coefficient at the shortest diffusion time measured and D_∞ as the water diffusion coefficient at the longest diffusion time measured.

transition at 0 °C for the HEMA-*co*-MMA copolymers suggests that these materials do not contain appreciable amounts of free or bulk water. This observation is also consistent with the calculations discussed in section 3.2, indicating that these polymers sorb ≤2 equiv of water per total equivalents of −OH and −O−.

We further used NMR diffusometry to investigate water molecule dynamics in the copolymers. In general, a one-dimensional (1D) ^{1}H NMR spectrum shows narrow spectral lines for species that experience fast molecular tumbling (dynamics), e.g., small molecules in liquid or solution. Broad spectral lines, however, correspond to species that experience slower molecular tumbling, e.g., proteins, polymer chains, solids, or small molecules confined inside another medium. Broad spectral lines correspond to much shorter NMR T_2 relaxation times, which represent the NMR signal decay lifetimes for these slow tumbling species. In NMR diffusometry experiments, these broad signals are partly or fully "weighted out" of the spectrum, as the signal decay lifetimes approach the length of certain delay times used in the diffusion pulse sequences.

Figure 5 shows a set of 1D NMR spectra for 0.5 mol/L NaCl hydrated HEA-*co*-EA 30:70 and HEMA-*co*-MMA 30:70. Figures 5A and 5B show data from pulse-acquire NMR experiments. Each spectrum shows two distinct ^{1}H NMR signals arising from polymer chains (broader signal = less mobile) and water molecules (narrow signal = more mobile). The 1D pulse-acquire spectrum of HEMA-*co*-MMA 30:70 (Figure 5B) was broader than that of HEA-*co*-EA 30:70 (Figure 5A) due to the slower segmental dynamics of the glassy HEMA-*co*-MMA copolymer compared to the rubbery HEA-*co*-EA copolymer.

DOI: 10.1021/acs.macromol.8b01830
Macromolecules 2018, 51, 9222−9233

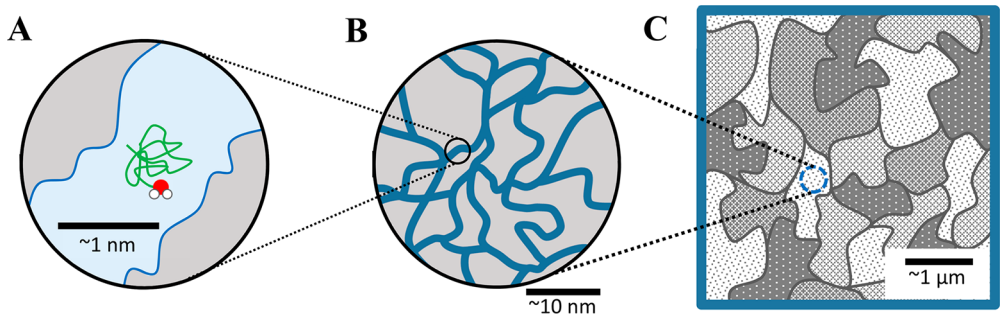

Figure 7. Diffusion through a heterogeneous polymer matrix over diffusion length scales l_d ranging from less than 1 nm to greater than 1 μm. Water molecules that diffuse within nanometer-scale hydrophilic pathways (A) over a mean-square displacement less than the radius R of the cavity or pathway ($l_d^2 = D\Delta < R^2$) will not show restricted diffusion behavior as the pathways are not tortuous on this length scale. This nanometer-scale "local" diffusion coefficient we define as D_{loc}. At larger length scale (B), we expect the pathways to be tortuous (indirect) paths. Average water diffusion on this length scale, $D_w[l_d]$, will be slower than what is observed in (A). At lengths ~1 μm and above (C), structural heterogeneities may reduce the observed water diffusivity relative to that observed at smaller length scales. As the diffusion length scale increases ($l_d^2 = D\Delta \gg R^2$), water diffusivity measured by NMR will approach the bulk diffusivity.

Figures 5C and 5D are 1D slices from the NMR diffusometry experiment. The broad signals from the polymers are completely attenuated (signal intensity greatly decreased) by the NMR pulse sequence due to their slow molecular motions and correspondingly short NMR relaxation time T_2. Furthermore, sorbed water motions in HEMA-*co*-MMA (Figure 5D) are substantially restricted (i.e., the T_2 relaxation time is shorter) relative to HEA-*co*-EA. This restriction of water molecule dynamics causes substantially stronger signal attenuation (and lower signal-to-noise ratio) in the diffusometry experiment compared that for HEA-*co*-EA.

3.5. Restricted Diffusion. We used NMR diffusometry to directly probe the restricted water molecule motions in the copolymers identified in the previous section. The water diffusion coefficient in the copolymers is length scale dependent, and NMR measurements of the water diffusion coefficient, D_w, as a function of diffusion time, Δ, show that water diffusivity decreases as the diffusion time increases (Figure 6). At longer length scales, the water diffusion coefficient appears to plateau to a value, D_∞, that we will consider to be equivalent to the water diffusion coefficient that could be measured via bulk transport property measurements.

The diffusion time, Δ, is related to the diffusion length, l_d, via the diffusion coefficient:

$$l_d = \langle r^2 \rangle^{1/2} = \sqrt{2D_w\Delta} \tag{7}$$

where $\langle r^2 \rangle^{1/2}$ is the root-mean-square distance that molecules travel during the NMR diffusometry experiment. D_w measurements for HEA-*co*-EA show that over short length scales ($l_d \approx$ 1 μm) diffusion behaviors are essentially equivalent for all of the HEA-*co*-EA copolymers (5×10^{-8} cm^2/s). As l_d increases to ≈2.7 μm, D_w values for all of the HEA-*co*-EA copolymers decrease by an order of magnitude (to 5×10^{-9} cm^2/s). A similar order of magnitude decrease in D_w is observed for HEMA-*co*-MMA copolymers when l_d increases from ≈0.5 to 1.2 μm.

These results show that the polymer environment imposes increased restrictions on water molecule diffusion as the diffusion length scale increases and that micrometer scale features within the polymer are at least partially driving this length-scale-dependent diffusion behavior.[28] Given that the water content of these polymers is relatively low (as discussed previously), it is reasonable to assume that diffusing water molecules must navigate a local nanometer-scale path, which is highly tortuous, among the hydrophilic segments of the polymer and other sorbed water molecules. Some of these pathways may lead to dead ends formed by clusters of hydrophobic polymer segments. The relevant length scales are illustrated in Figure 7. The subsequent discussion presents an interpretation and simple model of the experimental data framed in the context of molecular tortuosity.

3.6. Tortuosity. The tortuosity, $\mathcal{T}$, can be defined as the ratio of the water diffusion coefficient (at a specific diffusion length scale) to the long diffusion time (effectively bulk) water diffusion coefficient:

$$\mathcal{T}[l_d] = \frac{D_w[l_d]}{D_\infty} \tag{8}$$

where $D_w[l_d]$ is the water diffusion coefficient at a specific length scale, l_d, which is based on the experimental diffusion time. D_∞ is the water diffusion coefficient at infinite diffusion time (or length) and can be considered equivalent to what can be measured by bulk measurements across the membrane. In the context of the copolymers considered here, a value of $\mathcal{T}[l_d] = 1$ corresponds to a physical situation where the diffusivity at the specific length scale is equivalent to free diffusion with no restrictions (e.g., a free liquid). Because the water diffusion coefficient of the materials considered in this study tends to decrease as diffusion length increases (until reaching the plateau at long diffusion time), values of $\mathcal{T}[l_d] > 1$ are expected at relatively short diffusion lengths.

For the purpose of analyzing the diffusivity data for the copolymers, it is useful to define a "local-to-bulk" tortuosity, $\mathcal{T}_{L-B}$, and a "micrometer-to-bulk" tortuosity, $\mathcal{T}_{\mu-B}$:

$$\mathcal{T}_{L-B} = \frac{D_{loc}}{D_\infty} \tag{9}$$

$$\mathcal{T}_{\mu-B} = \frac{D_0}{D_\infty} \tag{10}$$

Both tortuosity values are defined relative to the measured water diffusion coefficient at long diffusion time/length, D_∞ (Δ = 750 ms or l_d = 2.5−3.0 μm). The measured water diffusion coefficient plateaued at $l_d \approx$ 2.7 μm in HEA-*co*-EA and $l_d \approx$ 1.1 μm in HEMA-*co*-MMA (Figure S1).

Comparing these two definitions of the tortuosity provides insight into the length scale that most influences the

DOI: 10.1021/acs.macromol.8b01830
Macromolecules 2018, 51, 9222−9233

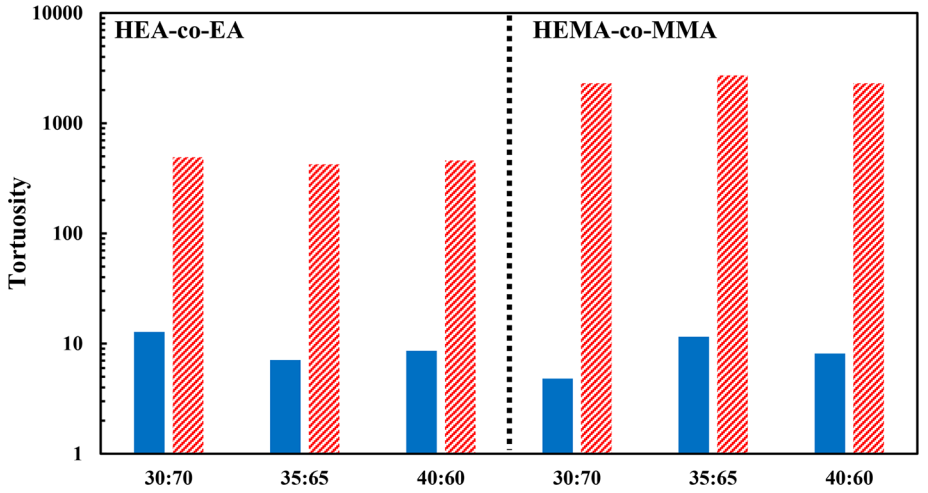

Figure 8. Local-to-bulk (eq 9, patterned bars) and micrometer-to-bulk (eq 10, solid bars) tortuosity values for HEA-*co*-EA and HEMA-*co*-MMA. All of the copolymers exhibit similar micrometer-to-bulk tortuosity, but the local-to-bulk tortuosity value for HEMA-*co*-MMA is larger than that for HEA-*co*-EA likely due to local nanoscale differences between the two copolymers.

differences in diffusion coefficients between the two copolymers. The local-to-bulk tortuosity $\mathcal{J}_{L-B}$ (eq 9) is the ratio of the water self-diffusion coefficient in bulk pure water, D_{loc}, and the water diffusion coefficient in the membrane at infinite diffusion time (or length), D_∞. Therefore, this definition of the tortuosity provides information about how polymer structure affects diffusivity over nanoscale to bulk length scales. The above $\mathcal{J}_{L-B}$ definition is analogous to the Mackie and Meares model for hindered diffusion where the local-to-bulk tortuosity can be related to the volume fraction of water in the polymer, i.e., K_w, as[47]

$$\mathcal{J}_{L-B} = \frac{D_{loc}}{D_\infty} = \frac{2 - K_w}{K_w^2} \tag{11}$$

Furthermore, the $\mathcal{J}_{\mu-B}$ (eq 10) is defined to describe the influence of micrometer-scale features of the polymer up to the bulk length scale. The definition of D_0 is established by a fixed time (for all samples) near the minimum measurable time (Δ = 20 ms). The diffusion length scale at this diffusion time is between 0.5 and 1 μm for the materials considered in this study. Therefore, the values of the water diffusion coefficient measured by NMR diffusometry and reported in Figure 6, represent micrometer-scale average water diffusion coefficients that are effectively averaged over a large path length relative to the molecular length scale. Note that the polymer chains will be separated by $\leq$1 nm given the ratio of water molecules to hydrophilic oxygen moieties in the material.

The value of D_{loc}, taken to be the water self-diffusion coefficient in bulk pure water, represents a limiting case of the largest water diffusion coefficient that could be observed in the copolymers. While the nanophase separation of the copolymers forms connected pathways for water to travel along, these pathways are also occupied by hydroxyl groups from the polymer chains. Given that the water content of the copolymers is low (~2 equiv of water per total equivalents of −OH and −O−, as discussed previously), the local diffusion behavior may be affected by local molecular and nanoconfinement effects.[57−59] This means that although the pathways are large enough for water to percolate through the entire thickness of the membrane, the local intermolecular interactions with the dipoles of the hydroxyls and esters of the polymer chains will affect the local diffusion behavior of water in these pathways. Future studies will consider more specifically the molecular interactions and nanoconfinement effects on water diffusion by measuring the activation energies of water diffusion in the copolymers.[57]

3.7. Morphology Models Related to Tortuosity Measurements. Comparing the $\mathcal{J}_{\mu-B}$ values for the copolymers shows that the HEA-*co*-EA and HEMA-*co*-MMA materials exhibit very similar diffusion coefficient behavior when considering micrometer-to-bulk scale structural effects (Figure 8). Over length scales ranging from the local (or nano) scale to the bulk scale, however, HEMA-*co*-MMA exhibits a factor of 5 greater tortuosity. This analysis suggests that transport property differences between the two copolymers arise due to differences in the materials that are present at the sub-micrometer scale. This result is reasonable given that the chemistry of the two copolymers is very similar, and no substantial evidence of phase separation was observed in the DSC thermograms. The critical sub-micrometer features that have a strong influence on water diffusivity are likely the result of nanometer-scale structures that differ between the two copolymers as a result of the different segmental dynamics of the backbones.

The Mackie and Meares model can be used to calculate the $\mathcal{J}_{L-B}$ value based solely on the water content of the polymer (eq 11). The Mackie and Meares model describes diffusion of molecules through obstacles, such as a network of polymer chains. In the context of the copolymers considered here, decreased water content (increased volume fraction of polymer in the hydrated material) causes a reduction in the diffusion coefficient relative to the value in bulk solution.[47] Equation 11 and the 0.5 mol/L K_w data from Table 1 can be used to calculate values for the local-to-bulk tortuosity. The Mackie and Meares model yields $\mathcal{J}_{L-B}$ tortuosity values (reported in the Supporting Information) ranging from 118 to 292. These values are roughly a factor of 2 or 3 less than the measured local-to-bulk tortuosity for HEA-*co*-EA, but they are an order of magnitude lower than that for HEMA-*co*-MMA. The Mackie and Meares model is a lattice-based model that describes how transport is hindered when polymer chains take up space.[47] The observation that the measured local-to-bulk tortuosity is greater than that calculated by the Mackie and Meares model

DOI: 10.1021/acs.macromol.8b01830
Macromolecules 2018, 51, 9222−9233

could suggest structural features, more significant in HEMA-*co*-MMA compared to HEA-*co*-EA, that preferentially restrict diffusion. For example, water transport in HEMA-*co*-MMA may be more restricted compared to HEA-*co*-EA if the structure of the tortuous transport pathways is more heterogeneous in the glassy copolymer.

Figure 9 illustrates a proposed model for the nanometer scale features that drive the water diffusivity differences between HEA-*co*-EA and HEMA-*co*-MMA. This model is similar to a model proposed by Kreuer for charged polymer systems used in fuel cell membranes.[21] The length scale between polymer chains may be smaller in the copolymers considered in this study compared to the charged polymers considered by Kreuer due to the low water content of the copolymers and the absence of charged groups.

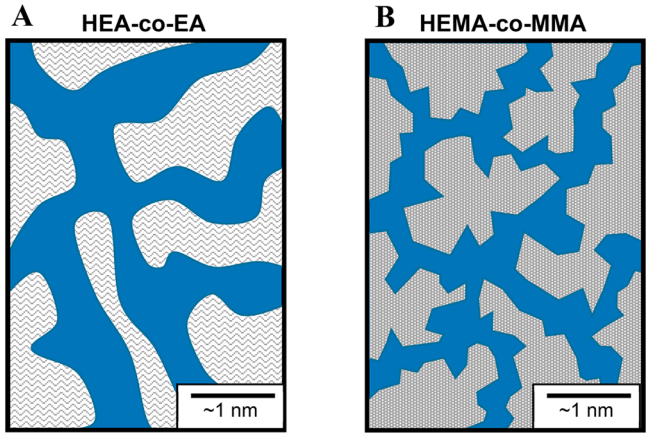

Figure 9. Illustration of the arrangement of hydrophilic and hydrophobic regions of the (A) HEA-*co*-EA and (B) HEMA-*co*-MMA membranes. Self-organization of hydrophilic functional groups present within the copolymers may create different geometries or dynamics of nanometer-scale transport pathways for the rubbery and glassy systems due to the differing arrangements and mobilities of the hydroxyl side chains from the HEA and HEMA moieties. We expect the hydroxyl side chains to extend into the pathways to interact with sorbed water, leading to wider pathways than one might expect for the observed ratio of sorbed water to hydrophilic moieties (roughly 2 equiv of sorbed water per equivalent of −OH and −O−).

In the copolymers, the hydrophilic side chains and ether groups (of the cross-linker) may self-organize into hydrophilic aggregates that define the critical nanoscale features discussed above. Faster HEA-*co*-EA backbone dynamics may allow polymer chains (and thus hydrophilic aggregates) to establish smoother and better connected transport pathways compared to the more rigid HEMA-*co*-MMA material. This physical picture agrees with the local-to-bulk tortuosity data in Figure 8 as more confined (and possibly more disconnected) pathways would be expected to exhibit smaller local diffusion coefficients and larger local-to-bulk tortuosity.

The hydrophobic polymer chain segments may form aggregates as well. These aggregates, which would tend to exclude water, could form "dead ends" and restrict transport pathways at larger length scales than the local effects described above. These restrictions would have the net effect of decreasing the average water diffusion coefficient at longer length scales (relative to the micrometer length scales) and explain the micrometer-to-bulk tortuosity values that are greater than unity. If these "dead ends" cluster together, micrometer-scale boundaries of limited transport pathway connectivity could form and separate regions of highly interconnected nanometer-scale hydrophilic pathways. These features are depicted in Figure 10. This larger length scale of transport pathway connectivity appears to be similar between the two copolymers, as the micrometer-to-bulk tortuosity is similar across all of the copolymers. This similarity likely results from the similar chemical structure and polymerization process used to prepare the copolymers.

3.8. Water/Salt Diffusion Properties. Salt diffusion is faster in the HEA-*co*-EA materials compared to the HEMA-*co*-MMA materials at comparable water content (Figure 11A). Slower diffusion in the more rigid HEMA-*co*-MMA material compared to the more flexible HEA-*co*-EA material is consistent with the idea that more rigid backbone polymers transport small molecules at a slower rate compared to more flexible backbone polymers,[8] as a result of the more tortuous pathways in HEMA-*co*-MMA (Figure 9).

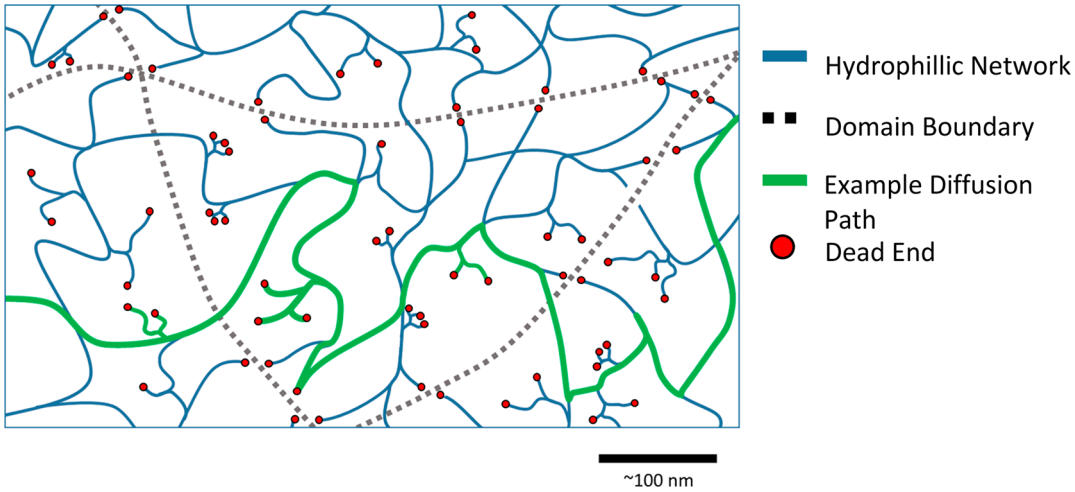

Figure 10. Proposed model of the heterogeneous hydrophilic network inside the HEA-*co*-EA and HEMA-*co*-MMA copolymers. Polymer domains are separated by clusters of "dead ends" where the hydrophilic network is interrupted by higher concentrations of hydrophobic chain segments. Continuous paths (green) allow water to transport through the membrane; however, dead ends along this path will restrict diffusion.

DOI: 10.1021/acs.macromol.8b01830
Macromolecules 2018, 51, 9222−9233

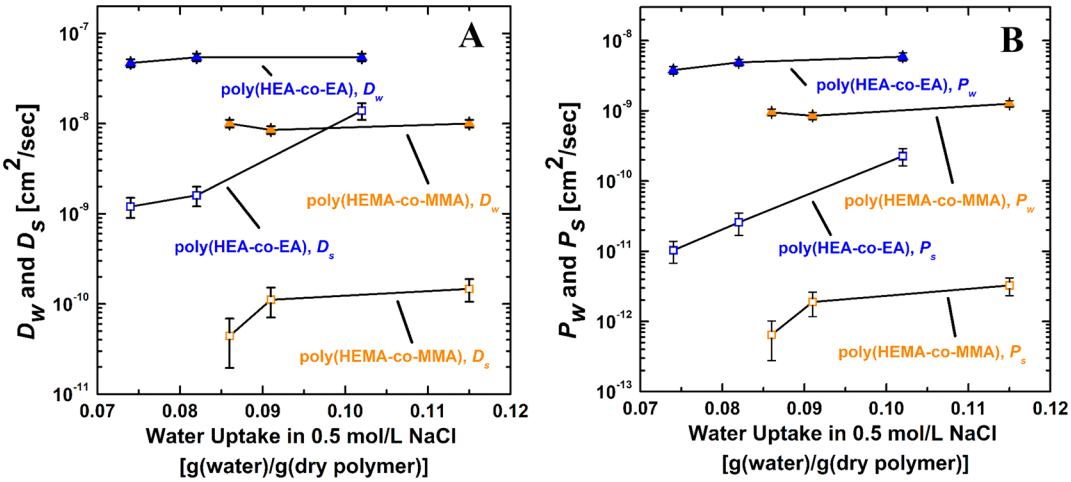

Figure 11. Water diffusivity, D_w (A), and permeability, P_w (B), data for poly(HEA-*co*-EA) (blue ▲) and poly(HEMA-*co*-MMA) (yellow ▲) copolymers and sodium chloride diffusivity, D_s (A), and permeability, P_s (B), data for poly(HEA-*co*-EA) (blue □) and poly(HEMA-*co*-MMA) (yellow □) copolymers as a function of water uptake. Water diffusivity data were measured via NMR. Salt diffusivity data were measured via kinetic desorption, where samples were characterized at 25 °C following equilibration in 0.5 mol/L aqueous NaCl. The water permeability was calculated as $P_w = D_w \times K_w$ using the measured diffusion and sorption (Table 1) coefficients. Salt permeability was calculated as $P_s = D_s \times K_s$ using the measured diffusion and sorption (Figures 3 and 12) coefficients. The uncertainty was taken as the standard deviation from the mean of three measurements.

3.9. Water/Salt Permeation Properties. Measured salt diffusivity and sorption coefficients were used to calculate salt permeability using the solution-diffusion model:[3,6,36,60]

$$P_s = K_s D_s \tag{12}$$

where P_s is the salt permeability, K_s is the salt sorption coefficient, and D_s is the effective salt diffusion coefficient.

While the salt sorption properties of the two copolymers were similar as a function of water content, the permeability properties were not similar as a function of water content. The more flexible HEA-*co*-EA materials have greater water and salt permeability values compared to the more rigid HEMA-*co*-MMA materials at equivalent water content (Figure 11B), and this observation is likely linked to the increased ability of water and salt to move through hydrophilic transport pathways in flexible, rubbery materials compared to rigid, glassy materials. These results are consistent with the idea that more flexible polymers have higher permeability properties compared to polymers with more rigid backbones,[8] and they are also consistent with the diffusivity data for the copolymers (Figure 11A).

Additionally, the water and salt permeability values, for both sets of copolymers, increase as copolymer water content increases. This observation is expected for hydrated polymers and underscores the need, in this study, to compare materials at comparable water content. Theoretical models including the Yasuda free volume model and the Mackie and Meares model predict this general behavior.[25,61]

3.10. Water/Salt Permeability and Diffusion Selectivity. The water permeability values can be divided by the salt permeability values (Figure 11) to calculate the ideal water/salt permeability selectivity. This ideal selectivity represents the rate of water permeation relative to salt permeation in situations where the permeability values are measured separately, and high selectivity values are desirable for desalination applications.[12,13] The more rigid HEMA-*co*-MMA materials exhibit greater permeability selectivity, P_w/P_s, compared to the more flexible HEA-*co*-EA materials at equivalent water content (Figure 12). Water/salt sorption selectivity does not depend significantly on backbone rigidity

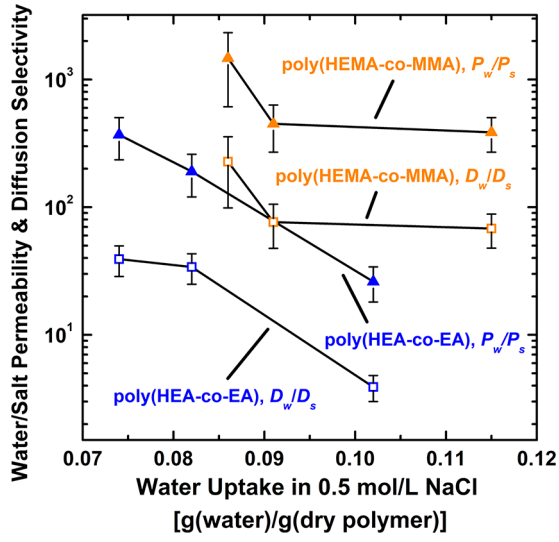

Figure 12. Water/salt permeability selectivity (P_w/P_s) for poly(HEA-*co*-EA) (blue ▲) and poly(HEMA-*co*-MMA) (yellow ▲) copolymers and water/salt diffusion selectivity (D_w/D_s) for poly(HEA-*co*-EA) (blue □) and poly(HEMA-*co*-MMA) (yellow □) copolymers as a function of water uptake.

in these copolymers (Figure 5), so the water/salt diffusion selectivity (D_w/D_s) of the rigid HEMA-*co*-MMA is greater than that of the flexible HEA-*co*-EA (Figure 12) in a manner similar to the permeability selectivity properties. Consistent with a free volume description of the transport process, the water/salt diffusion and permeability selectivity values decrease as polymer water content increases.[15,52] The results are consistent with established gas separation membrane structure−property relationships where rigid backbone polymers are generally more diffusion (or size) selective than flexible backbone polymers.[8,62]

DOI: 10.1021/acs.macromol.8b01830
Macromolecules 2018, 51, 9222−9233

Increased water/salt diffusivity and permeability selectivity in the glassy compared to rubbery copolymers may be due to greater tortuosity in HEMA-*co*-MMA compared to HEA-*co*-EA. Additionally, similar results (i.e., glassy polymers having greater selectivity and lower diffusivity compared to rubbery polymers) in gas separation membranes have been ascribed to the kinetics of the opening and closing of transient free volume elements, which facilitate transport, within the polymer.[8,63] While the relative contributions of these two factors are currently unknown for these materials, the data in Figure 12 suggest that glassy materials can offer greater water/salt diffusion selectivity (and, thus, water/salt permeability selectivity) compared to chemically similar rubbery materials.

4. CONCLUSIONS

We have investigated the influence of polymer backbone structure and dynamics on water and salt transport properties in two series of chemically similar, low water content, acrylate and methacrylate random copolymers. Micrometer-scale heterogeneities in both series of materials lead to water diffusivity, measured by NMR diffusometry, which decreases as the average diffusion length increases. We propose a model wherein nanometer-scale "dead ends" form micrometer-scale arrangements leading to this length-scale-dependent diffusion behavior in these materials. Additional morphological differences between the two copolymers on sub-micrometer length scales lead to increased water/salt selectivity properties, important for desalination applications, in the glassy versus rubbery materials (at equivalent water content). The results suggest that segmental dynamics influence water and salt transport properties at the nanoscale in low water content polymers where the majority of the water molecules are likely interacting with the polymer backbone. As such, glassy low water content polymers are expected to be more water/salt selective compared to rubbery materials at equivalent water content.

■ ASSOCIATED CONTENT

Supporting Information

The Supporting Information is available free of charge on the ACS Publications website at DOI: 10.1021/acs.macromol.8b01830.

Water content calculations; Mackie and Meares model calculations; diffusion coefficients as a function of diffusion length (PDF)

■ AUTHOR INFORMATION

Corresponding Author

*Ph 1-434-924-6248, e-mail geise@virginia.edu.

ORCID

Louis A. Madsen: 0000-0003-4588-5183

Geoffrey M. Geise: 0000-0002-5439-272X

Author Contributions

K.C. and A.K. are co-first authors.

Notes

The authors declare no competing financial interest.

■ ACKNOWLEDGMENTS

This research was supported in part by an Oak Ridge Associated Universities' Ralph E. Powe Junior Faculty Enhancement Award and by a 4-VA Collaborative Research Grant. This work was supported in part by the National Science Foundation under Awards DMR 1507764 and 1810194 and CBET 1752048.

■ REFERENCES

(1) Cohen, Y.; Semiat, R.; Rahardianto, A. A perspective on reverse osmosis water desalination: Quest for sustainability. *AIChE J.* **2017**, *63* (6), 1771−1784.

(2) Elimelech, M.; Phillip, W. A. The future of seawater desalination: Energy, technology, and the environment. *Science* **2011**, *333*, 712−717.

(3) Geise, G. M.; Lee, H.-S.; Miller, D. J.; Freeman, B. D.; McGrath, J. E.; Paul, D. R. Water purification by membranes: The role of polymer science. *J. Polym. Sci., Part B: Polym. Phys.* **2010**, *48* (15), 1685−1718.

(4) Fritzmann, C.; Löwenberg, J.; Wintgens, T.; Melin, T. State-of-the-art of reverse osmosis desalination. *Desalination* **2007**, *216* (1−3), 1−76.

(5) Shannon, M. A.; Bohn, P. W.; Elimelech, M.; Georgiadis, J. G.; Marinas, B. J.; Mayes, A. M. Science and technology for water purification in the coming decades. *Nature* **2008**, *452* (7185), 301−310.

(6) Geise, G. M.; Paul, D. R.; Freeman, B. D. Fundamental water and salt transport properties of polymeric materials. *Prog. Polym. Sci.* **2014**, *39* (1), 1−42.

(7) Kamcev, J.; Freeman, B. D. Charged Polymer Membranes for Environmental/Energy Applications. *Annu. Rev. Chem. Biomol. Eng.* **2016**, *7* (1), 111−133.

(8) Baker, R. W. *Membrane Technology and Applications*, 3rd ed.; Wiley: New York, 2012.

(9) Allegrezza, A. E.; Parekh, B. S.; Parise, P. L.; Swiniarski, E. J.; White, J. L. Chlorine resistant polysulfone reverse osmosis modules. *Desalination* **1987**, *64*, 285−304.

(10) Park, H. B.; Freeman, B. D.; Zhang, Z.-B.; Sankir, M.; McGrath, J. E. Highly chlorine-tolerant polymers for desalination. *Angew. Chem., Int. Ed.* **2008**, *47* (32), 6019−6024.

(11) Kimura, S. G. Reverse osmosis performance of sulfonated poly(2,6-dimethylphenylene ether) ion exchange membranes. *Ind. Eng. Chem. Prod. Res. Dev.* **1971**, *10* (3), 335−339.

(12) Park, H. B.; Kamcev, J.; Robeson, L. M.; Elimelech, M.; Freeman, B. D. Maximizing the right stuff: The trade-off between membrane permeability and selectivity. *Science* **2017**, *356* (6343), eaab0530.

(13) Werber, J. R.; Deshmukh, A.; Elimelech, M. The Critical Need for Increased Selectivity, Not Increased Water Permeability, for Desalination Membranes. *Environ. Sci. Technol. Lett.* **2016**, *3* (4), 112−120.

(14) Zhang, H.; Geise, G. M. Modeling the water permeability and water/salt selectivity tradeoff in polymer membranes. *J. Membr. Sci.* **2016**, *520*, 790−800.

(15) Geise, G. M.; Park, H. B.; Sagle, A. C.; Freeman, B. D.; McGrath, J. E. Water permeability and water/salt selectivity tradeoff in polymers for desalination. *J. Membr. Sci.* **2011**, *369* (1−2), 130−138.

(16) Freger, V. Swelling and morphology of the skin layer of polyamide composite membranes: An atomic force microscopy study. *Environ. Sci. Technol.* **2004**, *38*, 3168−3175.

(17) Zhang, X.; Cahill, D. G.; Coronell, O.; Mariñas, B. J. Absorption of water in the active layer of reverse osmosis membranes. *J. Membr. Sci.* **2009**, *331* (1), 143−151.

(18) Paddison, S. J.; Reagor, D. W.; Zawodzinski, T. A., Jr. High frequency dielectric studies of hydrated Nafion®. *J. Electroanal. Chem.* **1998**, *459* (1), 91−97.

(19) Hickner, M. A. Ion-containing polymers: New energy & clean water. *Mater. Today* **2010**, *13* (5), 34−41.

(20) Hickner, M. A. Water-mediated transport in ion-containing polymers. *J. Polym. Sci., Part B: Polym. Phys.* **2012**, *50* (1), 9−20.

DOI: 10.1021/acs.macromol.8b01830
Macromolecules 2018, 51, 9222−9233

(21) Kreuer, K. D. On the development of proton conducting polymer membranes for hydrogen and methanol fuel cells. *J. Membr. Sci.* **2001**, *185* (1), 29−39.
(22) Hickner, M. A.; Herring, A. M.; Coughlin, E. B. Anion exchange membranes: Current status and moving forward. *J. Polym. Sci., Part B: Polym. Phys.* **2013**, *51* (24), 1727−1735.
(23) Strathmann, H.; Grabowski, A.; Eigenberger, G. Ion-exchange membranes in the chemical process industry. *Ind. Eng. Chem. Res.* **2013**, *52* (31), 10364−10379.
(24) Chang, K.; Xue, T.; Geise, G. M. Increasing salt size selectivity in low water content polymers via polymer backbone dynamics. *J. Membr. Sci.* **2018**, *552*, 43−50.
(25) Yasuda, H.; Lamaze, C. E.; Ikenberry, L. D. Permeability of solutes through hydrated polymer membranes Part I. Diffusion of sodium chloride. *Makromol. Chem.* **1968**, *118*, 19−35.
(26) Callaghan, P. T. *Translational Dynamics and Magnetic Resonance: Principles of Pulsed Gradient Spin Echo NMR*; Oxford University Press: Oxford, NY, 2011.
(27) Mitra, P. P.; Sen, P. N.; Schwartz, L. M. Short-time behavior of the diffusion coefficient as a geometrical probe of porous media. *Phys. Rev. B: Condens. Matter Mater. Phys.* **1993**, *47* (14), 8565−8574.
(28) Hou, J.; Li, J.; Mountz, D.; Hull, M.; Madsen, L. A. Correlating morphology, proton conductivity, and water transport in polyelectrolyte-fluoropolymer blend membranes. *J. Membr. Sci.* **2013**, *448*, 292−299.
(29) Rumble, J. *CRC Handbook of Chemistry and Physics*, 98th ed.; CRC Press LLC: Boca Raton, FL, 2017.
(30) Geise, G. M.; Freeman, B. D.; Paul, D. R. Sodium chloride diffusion in sulfonated polymers for membrane applications. *J. Membr. Sci.* **2013**, *427*, 186−196.
(31) Zawodzinski, T. A.; Springer, T. E.; Davey, J.; Jestel, R.; Lopez, C.; Valerio, J.; Gottesfeld, S. A comparative study of water uptake by and transport through ionomeric fuel cell membranes. *J. Electrochem. Soc.* **1993**, *140* (7), 1981−1985.
(32) Ju, H.; Sagle, A. C.; Freeman, B. D.; Mardel, J. I.; Hill, A. J. Characterization of sodium chloride and water transport in crosslinked poly (ethylene oxide) hydrogels. *J. Membr. Sci.* **2010**, *358* (1), 131−141.
(33) Halliday, D.; Resnick, R.; Walker, J. *Fundamentals of Physics*, 7th ed.; Wiley: Hoboken, NJ, 2005.
(34) Luo, H.; Aboki, J.; Ji, Y.; Guo, R.; Geise, G. M. Water and salt transport properties of triptycene-containing sulfonated polysulfone materials for desalination membrane applications. *ACS Appl. Mater. Interfaces* **2018**, *10* (4), 4102−4112.
(35) Bevington, P. R.; Robinson, D. K. *Data Reduction and Error Analysis for the Physical Sciences*, 3rd ed.; McGraw-Hill: Boston, MA, 2003.
(36) Wijmans, J. G.; Baker, R. W. The solution-diffusion model: A review. *J. Membr. Sci.* **1995**, *107* (1), 1−21.
(37) Merten, U. *Desalination by Reverse Osmosis*; M.I.T. Press: Cambridge, MA, 1966.
(38) Pusch, W. Measurement techniques of transport through membranes. *Desalination* **1986**, *59*, 105−198.
(39) Xie, W.; Cook, J.; Park, H. B.; Freeman, B. D.; Lee, C. H.; McGrath, J. E. Fundamental salt and water transport properties in directly copolymerized disulfonated poly(arylene ether sulfone) random copolymers. *Polymer* **2011**, *52* (9), 2032−2043.
(40) Geise, G. M.; Willis, C. L.; Doherty, C. M.; Hill, A. J.; Bastow, T. J.; Ford, J.; Winey, K. I.; Freeman, B. D.; Paul, D. R. Characterization of aluminum-neutralized sulfonated styrenic pentablock copolymer films. *Ind. Eng. Chem. Res.* **2013**, *52* (3), 1056−1068.
(41) Atkins, P. W.; De Paula, J. *Atkins' Physical Chemistry*, 10th ed.; Oxford University Press: Oxford, NY, 2014.
(42) Xie, W.; Cook, J.; Park, H. B.; Freeman, B. D.; Lee, C. H.; McGrath, J. E. Fundamental salt and water transport properties in directly copolymerized disulfonated poly (arylene ether sulfone) random copolymers. *Polymer* **2011**, *52* (9), 2032−2043.
(43) Struik, L. C. E. *Physical Aging in Amorphous Polymers and Other Materials*; Elsevier Scientific Publishing Company: Oxford, NY, 1978.
(44) Seyler, R. J. *Assignment of the Glass Transition*; American Society for Testing & Materials: West Conshohocken, PA, 1994.
(45) Hou, J.; Li, J.; Madsen, L. A. Anisotropy and transport in poly(arylene ether sulfone) hydrophilic−hydrophobic block copolymers. *Macromolecules* **2010**, *43* (1), 347−353.
(46) Cussler, E. L. *Diffusion: Mass Transfer in Fluid Systems*, 3rd ed.; Cambridge University Press: Cambridge, NY, 2009.
(47) Mackie, J. S.; Meares, P. The diffusion of electrolytes in a cation-exchange resin membrane I. Theoretical. *Proc. R. Soc. London, Ser. A* **1955**, *232* (1191), 498−509.
(48) Geise, G. M.; Falcon, L. P.; Freeman, B. D.; Paul, D. R. Sodium chloride sorption in sulfonated polymers for membrane applications. *J. Membr. Sci.* **2012**, *423−424*, 195−208.
(49) Crank, J. *The Mathematics of Diffusion*, 2nd ed.; Clarendon Press: Oxford, NY, 1975.
(50) Geise, G. M.; Freeman, B. D.; Paul, D. R. Characterization of a sulfonated pentablock copolymer for desalination applications. *Polymer* **2010**, *51* (24), 5815−5822.
(51) Khare, A. R.; Peppas, N. Swelling/deswelling of anionic copolymer gels. *Biomaterials* **1995**, *16*, 559−567.
(52) Yasuda, H.; Ikenberry, L.; Lamaze, C. Permeability of solutes through hydrated polymer membranes. Part II. Permeability of water soluble organic solutes. *Makromol. Chem.* **1969**, *125* (1), 108−118.
(53) Hodge, I. M. Physical aging in polymer glasses. *Science* **1995**, *267* (5206), 1945−1947.
(54) Lutz, T. R.; He, Y.; Ediger, M. D.; Cao, H.; Lin, G.; Jones, A. A. Rapid poly(ethylene oxide) segmental dynamics in blends with poly(methyl methacrylate). *Macromolecules* **2003**, *36* (5), 1724−1730.
(55) Fox, T. G. J.; Flory, P. J. Second-order transition temperatures and related properties of polystyrene. I. Influence of molecular weight. *J. Appl. Phys.* **1950**, *21* (6), 581−591.
(56) Hiemenz, P. C.; Lodge, T. P. *Polymer Chemistry*, 2nd ed.; CRC Press LLC: Boca Raton, FL, 2007.
(57) Lingwood, M. D.; Zhang, Z. Y.; Kidd, B. E.; McCreary, K. B.; Hou, J. B.; Madsen, L. A. Unraveling the local energetics of transport in a polymer ion conductor. *Chem. Commun.* **2013**, *49* (39), 4283−4285.
(58) Kidd, B. E.; Forbey, S. J.; Steuber, F. W.; Moore, R. B.; Madsen, L. A. Multiscale lithium and counterion transport in an electrospun polymer-gel electrolyte. *Macromolecules* **2015**, *48* (13), 4481−4490.
(59) Kidd, B. E.; Lingwood, M. D.; Lee, M.; Gibson, H. W.; Madsen, L. A. Cation and anion transport in a dicationic imidazolium-based plastic crystal ion conductor. *J. Phys. Chem. B* **2014**, *118* (8), 2176−2185.
(60) Paul, D. R. Reformulation of the solution-diffusion theory of reverse osmosis. *J. Membr. Sci.* **2004**, *241* (2), 371−386.
(61) Paul, D. R. Relation between hydraulic permeability and diffusion in homogeneous swollen membranes. *J. Polym. Sci., Polym. Phys. Ed.* **1973**, *11* (2), 289−296.
(62) Yampol'skii, Y. P.; Pinnau, I.; Freeman, B. D. *Materials Science of Membranes for Gas and Vapor Separation*; John Wiley: Hoboken, NJ, 2006.
(63) Hofmann, D.; Fritz, L.; Ulbrich, J.; Schepers, C.; Böhning, M. Detailed-atomistic molecular modeling of small molecule diffusion and solution processes in polymeric membrane materials. *Macromol. Theory Simul.* **2000**, *9* (6), 293−327.

DOI: 10.1021/acs.macromol.8b01830
Macromolecules 2018, 51, 9222−9233